PMM Meeting
July 2015
Baltimore, MD

IPHEx Data Sets and Ongoing Studies

Anna Wilson[1], Jing Tao[1], Yajuan Duan[1], Malarvizhi Arulraj[1], Maria Cadeddu[3], Gregory Cutrell[1], Kyle Dawson[2], Markus Petters[2], Adrian M. Loftus[4], Douglas Miller[5], and Ana P. Barros[1]

1-Department of Civil and Environmental Engineering, Pratt School of Engineering, Duke University, NC
2-Department of Marine Earth and Atmospheric Science, North Carolina State University
3 – Climate and Atmospheric Science Department, Argonne National Laboratory, IL; 4- Goddard Space Flight Center, MD;
5-Department of Atmospheric Science, University of North Carolina at Asheville

1. Analysis – Disdrometers, Rain Gauges, H2F2P Trailer

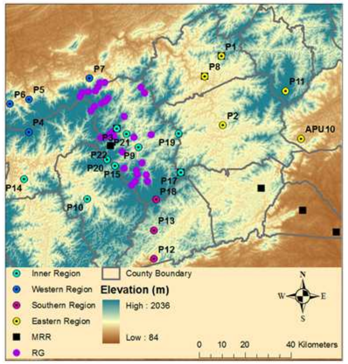

The dense disdrometer and rain gauge (RG) network shown at left was deployed in the Southern Appalachian Mountains (SAM) in order to investigate, at high resolution, the microphysical structure in this region throughout time-scales from diurnal to seasonal, as well as provide measures of precipitation DSD and accompanying rain rate at the surface to support ground-based radar retrieval algorithms (Barros et al., 2014). At right, subregional yearly averages recorded by the RGs illustrate interannual variability in this area. The bar plot shows the intra-ridge variability of the inner subregion.

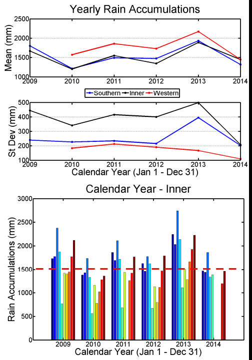

At right the diurnal cycle of 10 sensors that had less than one week of missing data for both months (Jan, in blue and July, in red) combined are presented. The parameters plotted are ratios of the mass weighted mean diameter (D_m) and its standard deviation (σ_m) to the regional average. Calculations were made for each 10s observation classified by the PARSIVEL disdrometer as liquid precipitation. DSDs were computed from raw drop observations using theoretical fall velocities including a density correction. In each region, the available stations show different effects. In the west, P4 is ~1.5 km higher than P7. PARSIVEL models 1 and 2 report large differences at P12. Over all regions, the Jan values show more spread. In general, we expect coalescence dominated regimes to show lower σ_m values, but in fog, that value may skew higher since the D_m value is pulled towards larger drops by the mass weighting. Below, the fog/rain frequency occurrence for P4 (West) and P3 (Inner) is plotted. The D_m curves at P4, which is commonly in the cloud deck, follow a similar pattern to the fog frequency curves, shown below, with an afternoon minimum and peak in the early morning.

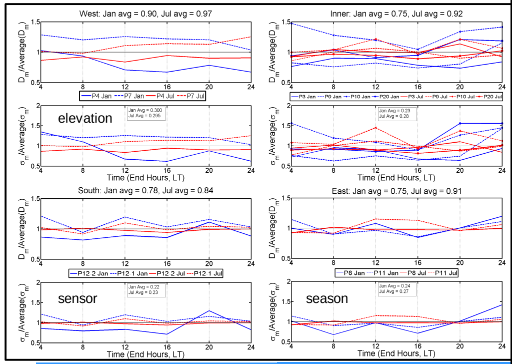

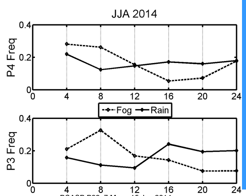

Below are DSDs measured at P9 (a location in the inner mountain region where the H2F2P (Haze to Fog to Precipitation) trailer was deployed for an extended period from August 2014-May 2015) and stratified by rain intensity (mm hr^{-1}, as reported by the disdrometers).

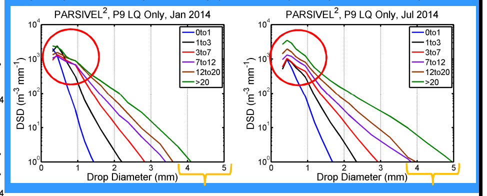

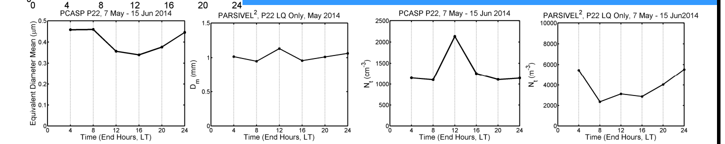

Above - parameters of the particle size distribution observed by the PCASP (Passive Cavity Aerosol Spectrometer) when it was not raining and the drop size distribution observed during rain events by the disdrometer, for the duration of the IOP at P22, during late spring/early summer. Below - the same parameters observed during a winter month (Jan) at the inner mountain location (P9) where the H2F trailer was stationed in that season. In the plots below, the PCASP was observing during both rain and non-rain conditions.
The evolution of the PSD → DSD is clearest in the total number concentration evolution. Midday peaks happen during both time periods in the PCASP (stronger in the warm season). The evolution is longer in the summer (~8 hours) than in the winter (~4 hours). Measures of the middle of the particle/drop size are higher in May-June than in January when smaller sizes are more dominant.

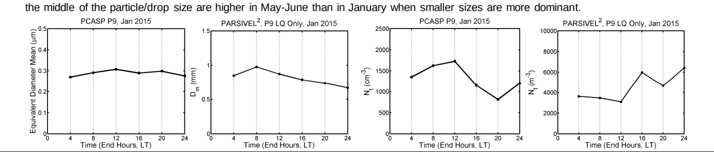

2. GPM DPR performance over the SAM

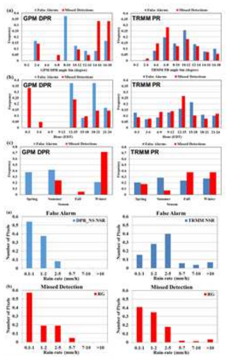

Figure 2.1 – Left panel: Histograms of FA and MD occurrences for one year of GPM 2ADPR near-surface rain rates (NSR) in the Southern Appalachians using the GSM PMM raingauge network as reference as a function of the viewing angle (a), time of day (b) and season of the year (c). Note the data are from total 135 GPM overpasses of normal scans (NS) in Ku-band during 03/2014 – 03/2015, hereafter DPR_NS (see Fig. 2.2). Right panel: Histograms of FA and MD occurrences for five years (2008-2013) of TRMM PR 2A25 V7 data in the Southern Appalachians using the same raingauge network as reference as a function of the viewing angle (a), time of day (b) and season of the year (c). Note mid-day light rainfall in the inner region dominates the MD statistics, whereas the statistics of FAs are strongly influenced by the presence of valley fog and orographic cap clouds in the inner region for all seasons (not shown here, see detailed error characterization in Duan et al., 2015).

Preliminary error analysis of GPM 2ADPR using one year (03/2014 – 03/2015) of overpasses over the SAM suggests similar behavior to PR 2A25 with strong seasonality of False Alarm (FA) and Missed Detection (MD) (Fig. 2.1c), though longer records are needed to consolidate the results. The seasonal cycle shows that FAs are more concentrated during warm season. However, MDs display a seasonal trend with a large proportion occurring during the cold season, which reveals its deficiency in detecting fog and low level clouds frequently present in the fall and winter seasons. Large viewing angles (Fig. 2.1a) can also contribute to this error. Despite the very limited sample size so far, the histograms of rainfall rates in Fig. 2.2 illustrate well the ambiguity and uncertainty in light rainfall estimates from GPM DPR.

Figure 2.2 – Histogram of FA and MD occurrences from DPR_NS NSR (left panel) and TRMM PR 2A25 NSR (right panel) and respective raingauge observations.

3. Climatology Study of Low-level Cloud and Fog in the SAM Using 8-year Satellite Observations and Modeling

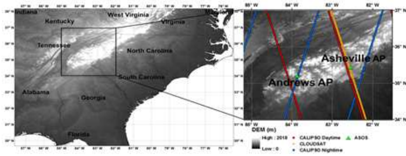

We present a multi-year climatology of the Low-level clouds (LLC) and fog with well-characterized uncertainties over the SAM using the satellite-based datasets (CALIPSO, CloudSat, and MODIS). A merging methodology developed to synergize CALIPSO and CloudSat data is intended to improve the quality of climate records of low cloud properties, with special emphasis on cloud base height (CBH) and top microphysical properties.

Figure 3.1 – Region of study in the SAM.

A. Comparison of Merged Satellite Observations with Ground Observations

D)		Ceilometer		
		Yes	No	Tot.
Satellite	Yes	71 (44%)	19 (11%)	90
	No	8 (5%)	66 (40%)	74
	Tot.	79	85	164

N)		Ceilometer		
		Yes	No	Tot.
Satellite	Yes	44 (34%)	22 (16%)	66
	No	30 (22%)	36 (28%)	66
	Tot.	74	58	132

During the study period (June 2006 – September 2014), there are 177 (Daytime) and 169 (Nighttime) overpasses for CALIPSO and 140 (Daytime) overpasses for CloudSat (see the study region in Figure 3.1). An assessment of the combined data was conducted with ceilometer cloud base height from ground observations (ASOS): Asheville and Andrews Airport, denoted as green triangles in Figure 3.1.

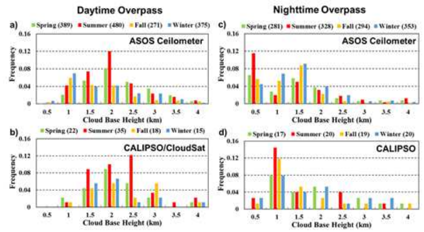

The contingency tables of 8-yr comparisons in Daytime (D) and Nighttime (N) are shown in the top panel. The figures in the middle panel show the probability distribution of (a) the first layer of CBHs detected from ground ceilometer around satellite overpass times (~ 14:50 local time) and (b) the combined satellite detections.

The climatology will be further developed through integration with results from WRF high-resolution simulations to aid in defining meteorological and time-of-day constraints in the interpretation of simulated satellite profiles through Goddard Satellite Data Simulator Unit (G-SDSU, Matsui et al., 2014).

B. Comparison of Satellite Observations to Model Simulations using G-SDSU

A 4-day WRF simulation (May 12 – May 16, 2014) during the IPHEx campaign was performed over the SAM, focusing on a rainfall event with afternoon convection mixed with fog and stratocumulus cloud. The performance of model results against satellite observations is expected to expand the geospatial coverage beyond narrow satellite sensor swaths and sampling that is inadequate to capture the diurnal cycle. The overarching goal is to infer a representation of seasonal and inter-annual variations of the vertical distribution of LWC and hydrometeors in orographic clouds and fog that vary spatially with landform toward contributing to a better diagnosis of the model microphysical parameterization of seeder-feeder interactions.

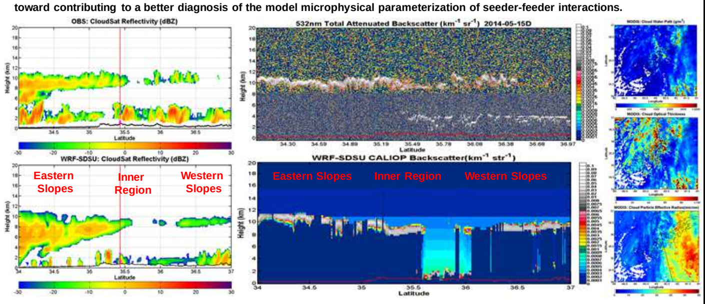

4. Multifrequency Radar Analysis

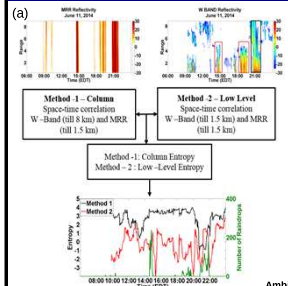

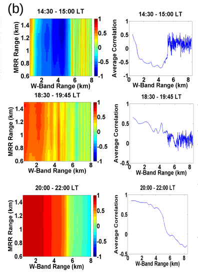

Figure 4.1: (a) Schematic of the algorithm to use Ka (MRR) and W (ACHIEVE) bands to classify low level (LL) and deep structure(DS) precipitation. (b) Space-time correlation structure and average correlation for two LL periods and a DS on June -11, 2014.

- **Time Period considered for analysis – IPHEx IOP (May 1 – June 15, 2014)**
- **Temporal resolution – 1 minute**
- **Vertical resolution:**
  - **W-Band: 25 m (0.5 km to 8.5 km)**
  - **Ka-Band: 50 m (50 m to 1.5 km)**
- **Method 2 is used for rain detection and Method 1 is used to classify the detected rain as low-level and deep structure.**
- **Ambiguity is around 20% for low-level events. Physical constraints will be incorporated next.**

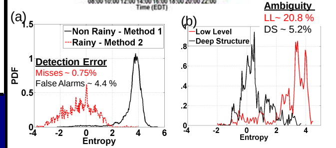

Figure 4.2: Probability Distribution Function (PDF) of: (a) Rainfall Detection (Method 1 for Non-Rainy Conditions and Method 2 for Rain events) (b) Rainfall Classification into Deep and Low-Level Structure using Method 1 (Column Entropy)

The algorithm was applied to CLOUDSAT CPR and TRMM PR reflectivities from 2007-2010. STAGE-IV rainfall data were used for identifying rainy events. The CPR reflectivities are consistent with actual rainfall along the overpass, but the TRMM 2A25 reflectivity data were not able to capture light rainfall structure except around 50-75.

Figure 4.3: Reflectivity profiles of (a) CLOUDSAT CPR (b) TRMM PR centered at (34N,84W) on February 4, 2010 14:58 LT. (c) Entropy compared with STAGE-IV precipitation.

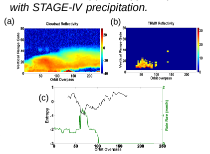

5. Hydrological Modeling

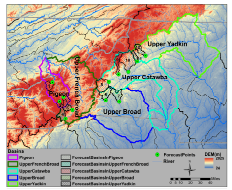

The operational hydrological forecast during IPHEx-IOP in May-June 2014 was dedicated to investigate the (flash) flood predictability in the southeast US on a daily basis in a complete operational environment, focusing on 12 headwater catchments in the Southern Appalachians with drainage size ranging from 71km² to 520 km² (see map at left). The Duke Coupled surface-groundwater Hydrology Model (DCHM) was utilized for flood forecasting combining QPFs (Quantitative Precipitation Forecasts) provided by the NASA-Unified Weather Research and Forecasting (NU-WRF) model, and multiple radar-based QPEs (Quantitative Precipitation Estimates) from NSSL Q3/MRMS (Multi-Radar/Multi-Sensor) and NCEP/EMC StageIV radar products. The QPEs were operationally used to produce hydrological hindcasts for the previous day. The final states from those hindcasts were used as initial conditions in the hydrological forecast for the current day. The operational forecast/hindcast results during the campaign caught all flash flood events with large lead times of up to 6 hours. In subsequent analyses, QPFs were improved through assimilating satellite observations into the NU-WRF, ingesting both ground and satellite radar-based QPEs as well as raingauge observations, and discharge observations into the DCHM using three data assimilation techniques (i.e. EnKF, EnKS and AEnKF), for advancing flood forecasting skills in the operational mode. The added value of this assimilation was assessed for the different datasets (Tao and Barros, 2015). Figure 5a shows the hydrological forecasts for the entire IPHEx IOP in the Upper Catawba (~ 515 km²).

*Below: Fig 5.1 **a)** Operational 24-hour lead-time streamflow forecasts using NU-WRF rainfall forecasts. Initial conditions derived from hindcasts using the NOAA Q3 (MW) rainfall; **b)** cumulative rainfall for the May 15th event from different products. Spatial resolution: NU-WRF and Q3 - 1 km; StageIV - 4km, and IMERG - 10km.*

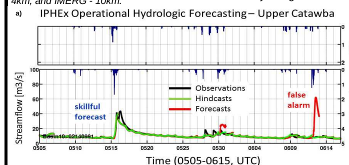

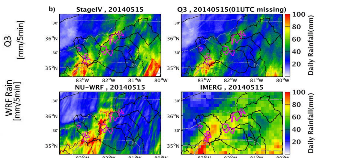

Right – Forecast/Hindcast results on May 15, 2014 using the original Q3 and the adjusted Q3 data (Q3+_). The grey lines are simulation ensemble members using 50 rainfall replicates drawn from normal distributions within the 70% and 95% confidence interval (CI) of the regression model.*
Below - Forecast results with the best DA scheme identified for each basin (i.e. respectively EnKS_AF15min_TW2hr for Basin01, EnKS_AF15min_TW1hr for Basin02, and AEnKF_AF15min_TW2hr for Basin03) with short to longer lead times (6hr to 15hr). The forecasting time is marked at the time-axis by the dot with the same color as the forecast result. *This work suggests that to achieve optimal skill, a "DA model climatology" study should be conducted.*

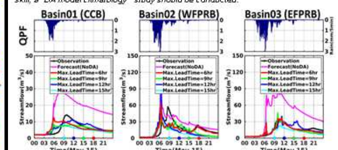

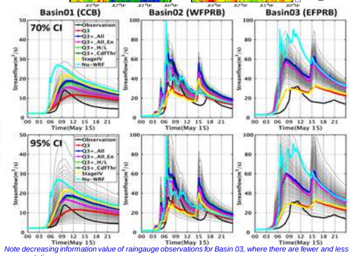

Note decreasing information value of raingauge observations for Basin 03, where there are fewer and less representative gauges.

Note that 6-hour lead time is much larger than time to peak for these small headwater basins.

6. References and Acknowledgements

1. Barros, A. P., Petersen, W., Schwaller, M., Cifelli, R., Mahoney, K., Peters-Liddard, C., and Zipser, E. (2014). NASA GPM-Ground Validation: Integrated Precipitation and Hydrology Experiment 2014 Science Plan. Duke University, Durham, NC, doi, 10, G8CC0XMR.
2. Duan, Y., Wilson, A. M., and Barros, A. P. (2015). Scoping a field experiment: error diagnostics of TRMM precipitation radar estimates in complex terrain as a basis for IPHEx2014. *Hydrology and Earth System Sciences*, 19(3), 1501-1520.
3. Matsui, T., Santanello, J., Shi, J. J., Tao, W.-K., Wu, D., Peters-Lidard, C., Kemp, E., Chin, M., Starr, D., Sekiguchi, M., Aires, F. (2014) Introducing multisensor satellite radiance-based evaluation for regional Earth System modeling. *J. Geophys. Res.*: Atmos., 119:10.1002/jgrd.v119.13, 8450-8475.
4. Tao, J., and Barros, A. P. (2014), Coupled prediction of flood response and debris flow initiation during warm- and cold-season events in the Southern Appalachians, USA, *Hydrology and Earth System Sciences*, 18(1), 367-388.

– **Acknowledgments: This research is supported by the NASA PMM Program.**